Norwegian
Meteorological
Institute

No. 1/2025
ISSN 2387-4201
Climate

METreport

2.5 km future climate projections for Svalbard under the high emission scenario SSP5-8.5

PCCH-Arctic Report No. 7

Oskar A. Landgren, Julia Lutz, Ketil Isaksen

[Classification: open]

Title	Date
2.5 km future climate projections for Svalbard under the high emission scenario SSP5-8.5	27.05.2025
Section Climate	**Report no.** No. 1/2025
Author(s) Oskar A. Landgren, Julia Lutz, Ketil Isaksen	**Classification** ● Free ○ Restricted
Client(s) Norwegian Research Council	**Client's reference**

Abstract

Svalbard is one of the fastest warming regions on the planet. In this report we present climate simulations produced with the regional climate model HCLIM-AROME, using input from two global climate models, MPI-ESM1-2-LR and NorESM2-MM, both from the CMIP6 ensemble and following the high emission scenario SSP5-8.5 for years 1991–2070, as well as the reanalysis ERA5 for years 2000–2023. The fine scale domain covers Svalbard in 2.5 by 2.5 km grid cells and output data is archived at 3-hourly temporal resolution. This report presents an overview of the dataset, including initial evaluation and information on how to access the data.

Compared to the CARRA dataset, the HCLIM run based on MPI-ESM1-2-LR demonstrates for a set of climate indices derived from temperature that the model captures spatial patterns well, though it tends to overestimate warm days while underestimating frost days. Precipitation-related indices indicate that the model reproduces the frequency and intensity of wet days reasonably, although it tends to over-represent very heavy precipitation events.

For 2041–2070, simulations project significant warming (around 3.2 °C in annual mean relative to 1991-2020) and moderate increases in precipitation (about 6 % overall), with the strongest temperature rise in winter (around 4.9 °C) linked to sea ice retreat. Precipitation is expected to intensify, with more frequent wet days and more precipitation on these days across Svalbard.

Keywords

climate, Svalbard, future climate change, regional climate modelling, dynamical downscaling

Disciplinary signature
Helene Birkelund Erlandsen

Responsible signature
Harald Schyberg

Meteorologisk institutt
Meteorological Institute
Org.no 971274042
post@met.no

Oslo
P.O. Box 43 Blindern
0313 Oslo, Norway
T. +47 22 96 30 00

Bergen
Allégaten 70
5007 Bergen, Norway
T. +47 55 23 66 00

Tromsø
P.O. Box 6314,
Langnes
9293 Tromsø, Norway
T. +47 77 62 13 00

www.met.no

Table of contents

1 Introduction

Over the past decades, Svalbard has experienced a rate of warming significantly higher than the global average (Isaksen et al., 2022a). This rapid climate change has led to profound environmental shifts such as shorter snow seasons (Hanssen-Bauer et al., 2019), thawing permafrost (e.g., Grünberg et al., 2024; Isaksen et al., 2022b), decreasing sea ice (Onarheim et al., 2018), and melting glaciers (van Pelt et al., 2021). These changes pose considerable challenges not only for ecosystems (e.g., Pedersen et al., 2022) but also for local infrastructure (Jaskólski et al., 2018; Streletskiy et al., 2023), increasing the need for precise and region-specific climate information.

To provide relevant climate insights at a local scale in a geographically diverse region like Svalbard, high-resolution meteorological data is essential. Many climate change impacts, such as thawing of permafrost, unfold over decades, requiring multi-decadal simulations to capture slow but critical processes. However, previous regional climate simulations for Svalbard have been limited by either coarse spatial resolution (e.g., Arctic CORDEX at ~50 km) or short time spans (e.g., two 30-year periods in Dobler et al., 2020).

In this report, we present an 80-year dataset of continuous climate simulations at a high spatial resolution of 2.5 x 2.5 km. This dataset offers valuable resources for understanding long-term climate trends and their implications for Svalbard's environment and infrastructure.

2 Method

2.1 Model setup

The regional climate model HARMONIE-Climate (HCLIM; Belušić et al., 2020; Wang, 2024) was employed to dynamically downscale future climate simulations, providing an internally physically consistent fine-scale representation of local meteorological variables based on coarser global model output. Input data were derived from two different global earth system models participating in the sixth generation of the Coupled Model Intercomparison Project (CMIP6), specifically ScenarioMIP simulations (O'Neill et al., 2016): MPI-ESM1-2-LR (Mauritsen et al., 2019) and NorESM2-MM (Seland et al., 2020). Both were run under the high-emission scenario SSP5-8.5. While this scenario is more extreme than the more commonly used SSP3-7.0, we motivate our choice of SSP5-8.5 using the following arguments:

- A strong climate change signal makes it possible to study climate change effects in a more statistically robust way, as it can more easily be separated from internal variability.

- For many purposes it can be possible to represent climate change from lower emission scenarios using an earlier period from a high scenario simulation.

Meteorologisk institutt
Meteorological Institute
Org.no 971274042
post@met.no

Oslo
P.O. Box 43 Blindern
0313 Oslo, Norway
T. +47 22 96 30 00

Bergen
Allégaten 70
5007 Bergen, Norway
T. +47 55 23 66 00

Tromsø
P.O. Box 6314,
Langnes
9293 Tromsø, Norway
T. +47 77 62 13 00

www.met.no

- Also in the Climate in Svalbard 2100 report, the corresponding high emission scenario was used (RCP8.5 in that generation of simulations), following a Norwegian government white paper on climate change adaptation (Meld. St. 33 (2012–2013)) stating that for precautionary reasons high emission climate projections should be used.

Regarding the two selected global models, following Levine et al. (2024), these two reflect contrasting future climate storylines in the Arctic during the biologically active summer half of the year. NorESM2-MM depicts strong Arctic amplification (enhanced warming in the Arctic relative to the rest of the world) but exhibits comparatively weaker warming in the Barents-Kara Sea region. On the other hand, MPI-ESM1-2-LR simulates a relatively weaker Arctic amplification overall but a pronounced warming signal in the Barents-Kara Sea region.

Due to the coarse resolution of the global models (horizontal grid spacing of ~200 km for MPI-ESM1-2-LR and ~100 km for NorESM2-MM), a nested modeling approach was applied. The outer domain, covering the Norwegian and Barents Seas, has a 12 km spatial resolution and was run with hydrostatic HARMONIE-ALADIN physics. The inner domain, covering Svalbard at a finer 2.5 km resolution, was simulated with nonhydrostatic HARMONIE-AROME physics. These model domains are illustrated in Fig. 1. The high-resolution Svalbard domain is particularly relevant for studying both human activities and ecological processes, as it more accurately captures local variations in temperature and precipitation, especially in steep valleys and fjords.

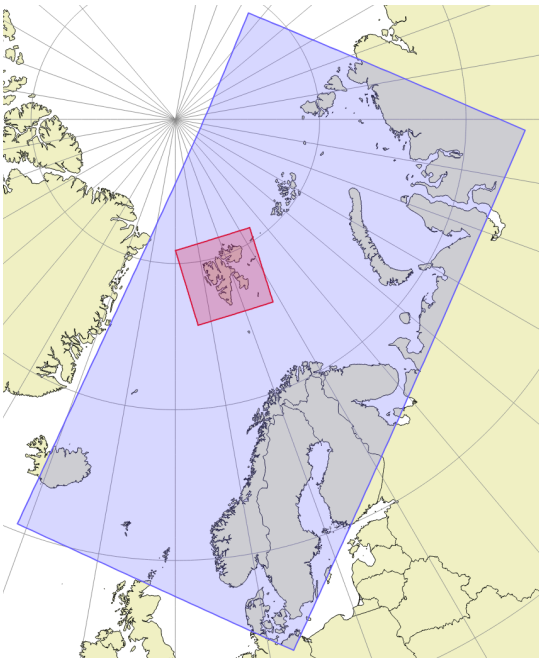

Figure 1 The two simulation domains used in the study: an outer domain (blue) with 12 km horizontal resolution with 181 x 349 grid cells and an inner domain (red) covering Svalbard at 2.5 km resolution with 229 x 229 grid cells.

A more detailed analysis was conducted for selected grid cells representative of Ny-Ålesund and Longyearbyen/Adventdalen (Fig. 2). In addition to future projections, an evaluation simulation was performed using the fifth generation ECMWF Reanalysis (ERA5; Hersbach et al., 2020).

For this evaluation, the downscaling was done directly from the ~25 km ERA5 data to the 2.5 km inner domain, without an intermediate nesting step. An overview of all simulations is provided in Table 3. For all simulations, the HCLIM version used was cycle 43 (cy43), which includes the land surface model SURFEX (version 8.1; Le Moigne, 2018). SURFEX incorporates the 12-layer ISBA-ES snow scheme (Boone, 2002).

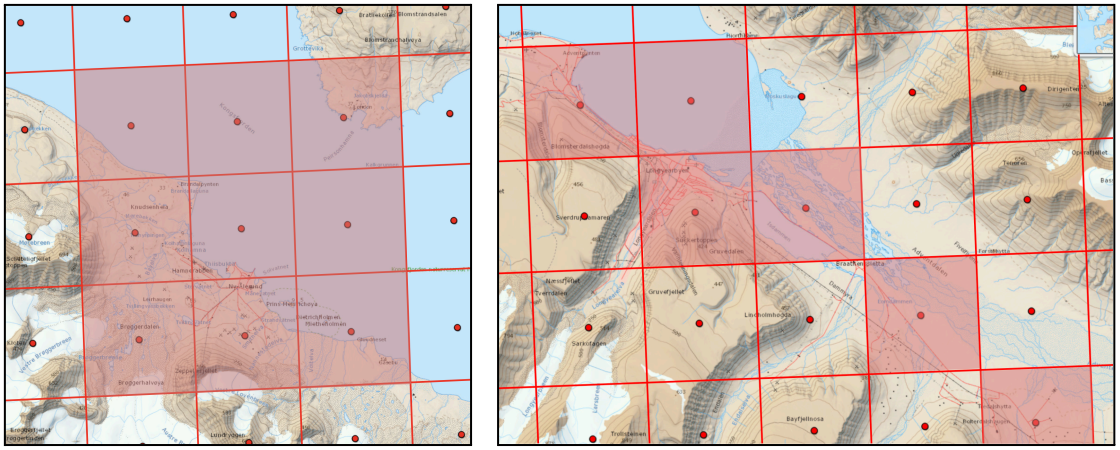

Figure 2 Maps showing the 2.5 x 2.5 km grid cells around Ny-Ålesund (*left*) and Longyearbyen-Adventdalen (*right*), with a selection of grid cells shaded in red used for further analysis (9 and 6 grid cells, respectively). Map data from TopoSvalbard, courtesy of the Norwegian Polar Institute.

3 Key results

3.1 Evaluation for the reference period

We begin by comparing the simulations with the Copernicus Arctic Regional Reanalysis (CARRA; Schyberg et al., 2020) for the period 1991–2020, the reference period in this report. CARRA provides data for two partially overlapping domains covering Svalbard. For this analysis, we use data from the eastern domain, as it places Svalbard farther from the domain edge, reducing potential boundary effects. Differences in annual mean temperature and total precipitation between the simulations and CARRA are presented in Figures 3 and 4.

Figure 3 shows the mean annual temperature from CARRA alongside differences from simulations based on ERA5, MPI-ESM and NorESM. Because the ERA5-based simulation starts in 2000, comparisons with CARRA use the 2000–2020 period for ERA5, and the full 1991–2020 period for the other simulations. Over land, both the ERA5- and MPI-ESM-based simulations are slightly colder than CARRA over Spitsbergen, while showing a slight warm bias in the eastern regions. The ERA5-based simulation exhibits the strongest warm bias over the

Meteorologisk institutt
Meteorological Institute
Org.no 971274042
post@met.no

Oslo
P.O. Box 43 Blindern
0313 Oslo, Norway
T. +47 22 96 30 00

Bergen
Allégaten 70
5007 Bergen, Norway
T. +47 55 23 66 00

Tromsø
P.O. Box 6314,
Langnes
9293 Tromsø, Norway
T. +47 77 62 13 00

www.met.no

ice-covered Barents Sea in the eastern part of the domain, likely due in part to the lack of snow cover on sea ice in ERA5, which can result in higher winter temperatures (Batrak & Müller, 2019).

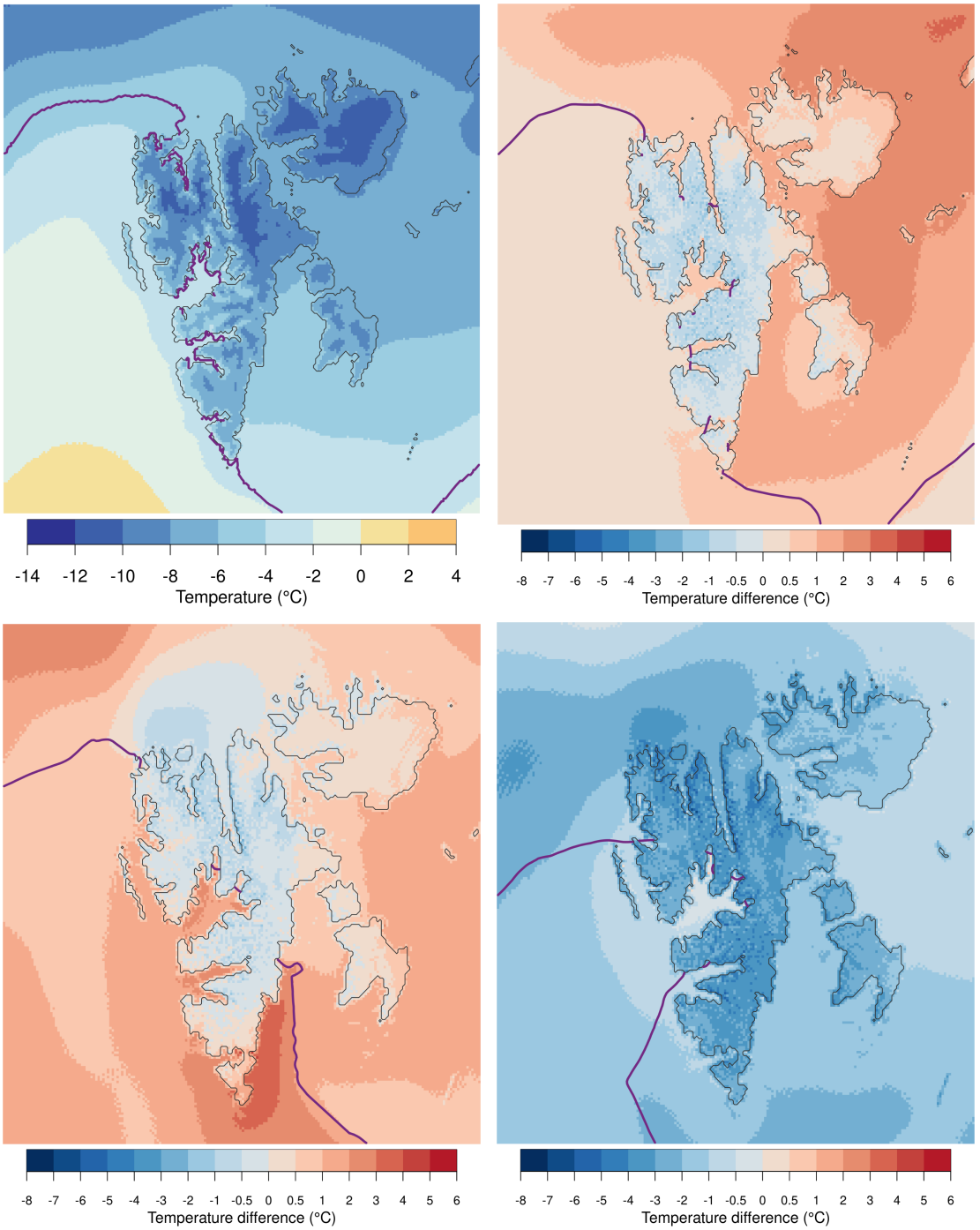

Figure 3 Mean annual 2-metre temperature (°C). *Top left*: CARRA reanalysis 1991–2020. *Top right:* Difference between HCLIM43-AROME simulation, driven by ERA5, and CARRA, 2000–2020. *Bottom left*: Difference between HCLIM43-AROME, driven by MPI-ESM1-2-LR, and CARRA, 1991–2020. *Bottom right*: Difference between HCLIM43-AROME, driven by NorESM2-MM, and CARRA, 1991–2020. The dark magenta lines indicate the average location of the sea ice edge, defined as the 15 % sea ice concentration in the annual mean.

The MPI-ESM-based simulation is slightly warmer than CARRA, particularly over ocean, whereas the NorESM-based simulation is generally colder. While this may be a general bias in this region for this model, it also contributes to placing NorESM among the models with weak warming in the Barents-Kara Sea region in the storylines of Levine et al. (2024), manifesting a complementary future scenario with quite different development in this region. In terms of sea ice concentration (illustrated by the magenta lines in Fig. 3), the MPI-ESM-based simulation aligns better with CARRA but extends farther east in the southern part of the domain. In contrast, the simulation based on NorESM has a considerably larger fraction of the domain covered in sea ice, which places the sea ice edge farther south in the north and significantly farther west in the southern part of the domain.

In the HCLIM model system, sea ice concentration is not explicitly modelled but is instead interpolated from the global model used as input. Since Svalbard is located near the sea ice edge, any model biases in the representation of sea ice in the driving GCM can substantially affect local temperatures. This effect is particularly evident in Fig. 3, where ocean temperatures near the southern tip of Svalbard are 4–5 °C higher in the MPI-ESM1-2-LR-based simulation compared to CARRA.

Figure 4 follows the same structure as Figure 3 but focuses on total annual precipitation. As expected, the ERA5-based simulation closely reproduces results from CARRA, with only a small wet bias along the coasts. While the central fjords receive slightly less precipitation than in CARRA, these areas are inherently very dry, meaning that even small absolute differences can appear large in relative terms. The MPI-ESM-based simulation is drier than CARRA over the ocean but slightly wetter over land, especially over the southeastern part of Svalbard, where biases reach up to 50 %. In contrast, the NorESM-based simulation is generally drier, with biases of 30–50 % over land.

In all simulations, the dry bias along the domain boundary, particularly in the south, is likely due to lateral spin-up effects in the microphysics scheme. As moist air is advected into the domain, it takes time for rain droplets to form, leading to reduced precipitation. This effect may also contribute to the wet bias over land in the MPI-ESM-driven simulation, because the increased availability of moisture could result in higher precipitation amounts than would be expected in a larger domain. However, expanding the domain was deemed computationally prohibitive. It is important to note that, in absolute terms, precipitation over the ocean and sea ice is significantly lower than over land, where steep mountainous terrain enhances precipitation through orographic effects. The negative bias over ocean and sea ice is therefore not as large in absolute terms.

In the following section, we look closer at some climate indices derived from temperature and precipitation. As with annual mean temperature and precipitation, we compare the simulations to CARRA. However, from here onwards we focus on the MPI-ESM-based simulation (rather than the NorESM-based one), as its climate in the reference period follows more closely the CARRA reference dataset, including a more realistic representation of the sea ice edge.

Meteorologisk institutt
Meteorological Institute
Org.no 971274042
post@met.no

Oslo
P.O. Box 43 Blindern
0313 Oslo, Norway
T. +47 22 96 30 00

Bergen
Allégaten 70
5007 Bergen, Norway
T. +47 55 23 66 00

Tromsø
P.O. Box 6314,
Langnes
9293 Tromsø, Norway
T. +47 77 62 13 00

www.met.no

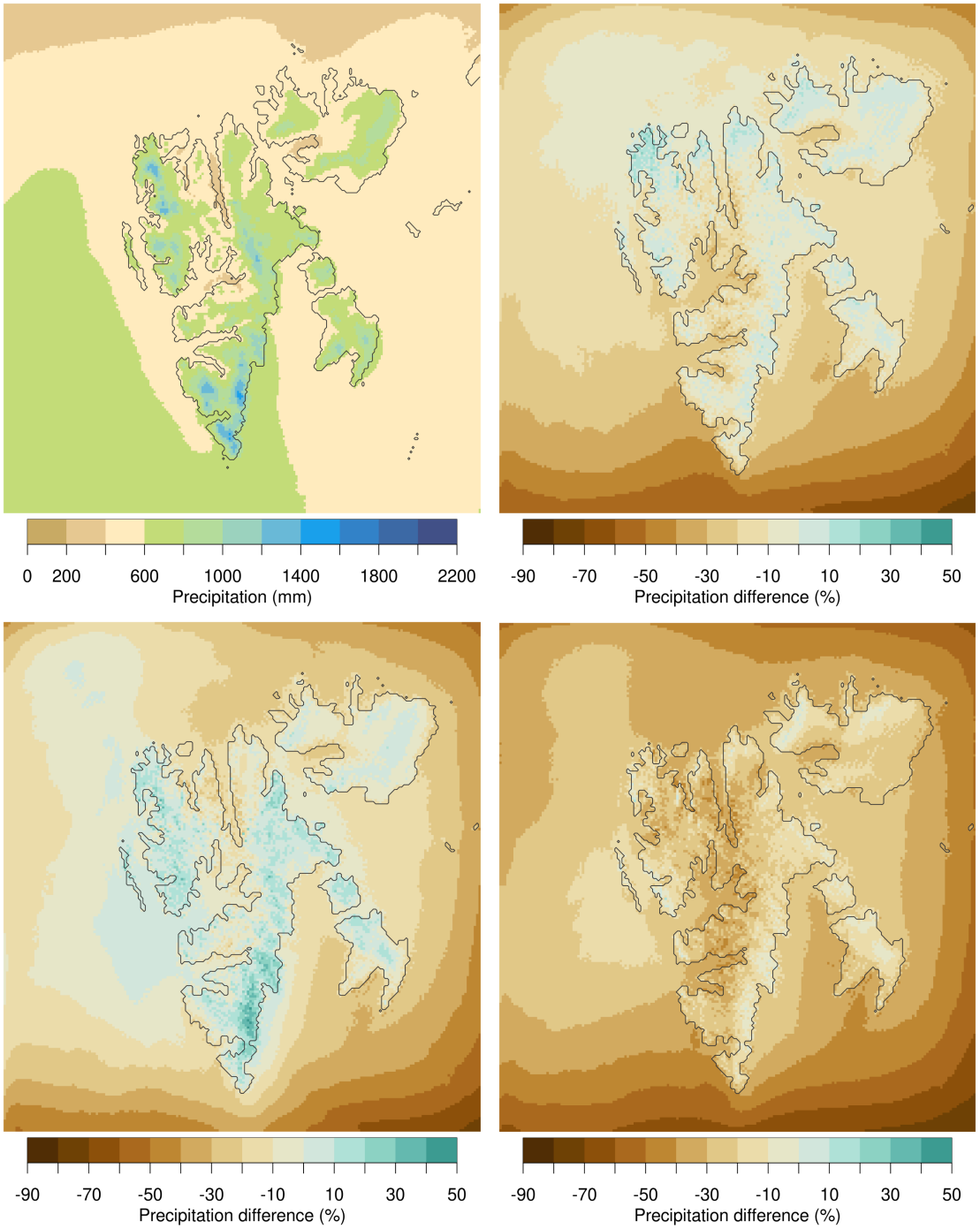

Figure 4 Mean annual precipitation (mm in first panel, % in others). *Top left*: CARRA, 1991–2020. *Top right:* Difference between HCLIM43-AROME simulation, driven by ERA5, and CARRA, 2000–2020. *Bottom left*: Difference between HCLIM43-AROME, driven by MPI-ESM1-2-LR, and CARRA, 1991–2020. *Bottom right*: Difference between HCLIM43-AROME, driven by NorESM2-MM, and CARRA, 1991–2020.

Climate indices derived from temperature

Figure 5 presents the mean annual number of growing days (Førland et al., 2004) derived from CARRA for 1991–2020, along with the difference between the MPI-ESM-based simulation and CARRA. Growing days are defined as days on which the mean daily temperature exceeds 5 °C.

In CARRA, most growing days are concentrated along the western coast of Spitsbergen, particularly around Isfjorden and Van Mijenfjorden, where the growing season lasts approximately two to three months. Overall, the simulation agrees well with CARRA across most of Svalbard, though it slightly overestimates the number of growing days. In some southern coastal areas, the simulated growing season is up to two months longer, which coincides with the model's overestimation of mean annual temperature in this region.

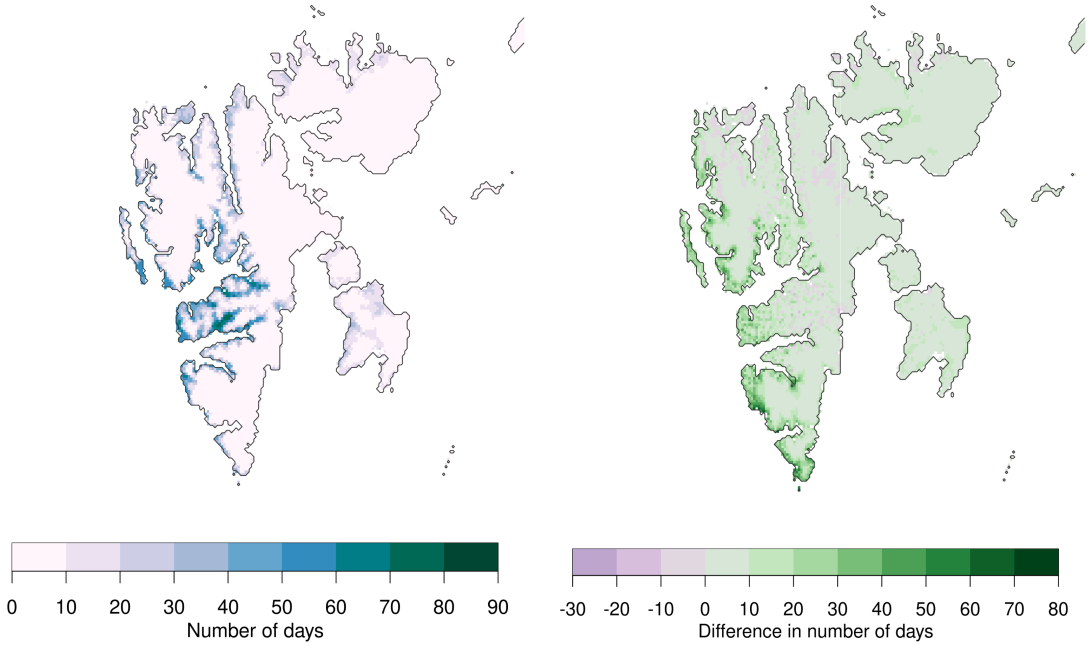

Figure 5 *Left*: Mean annual number of days with daily mean temperature > 5 °C for 1991–2020, derived from CARRA. *Right*: Difference in the mean annual number of days with T_{mean} > 5 °C between HCLIM43-AROME (driven by MPI-ESM1-2-LR) and CARRA.

The left panel of Figure 6 shows the mean annual number of days with a daily mean temperature above 10 °C for 1991–2020, based on CARRA. The right panel displays the difference between the MPI-ESM-based simulation and CARRA for the same period. In CARRA, such days are rare and mostly confined to coastal areas around Isfjorden and Van Mijenfjorden. However, the simulation overestimates their occurrence, especially along the western coast of Spitsbergen, where the number of warm days is higher by several days.

The number of frost days, defined as days on which the minimum temperature falls below 0 °C, is presented in Figure 7. As in previous figures, the left panel shows CARRA data for 1991–2020, while the right panel displays the difference between the MPI-ESM-based simulation and CARRA. Given Svalbard's Arctic climate, the number of frost days is unsurprisingly high, ranging from around 250 days in coastal areas to over 300 days in inland regions. The highest values occur in the northern and northeastern glacial areas. Overall, the simulation underestimates the number of frost days, particularly in the south, where the difference can exceed 60 days. This is likely explained by the difference in sea ice concentration

Meteorologisk institutt
Meteorological Institute
Org.no 971274042
post@met.no

Oslo
P.O. Box 43 Blindern
0313 Oslo, Norway
T. +47 22 96 30 00

Bergen
Allégaten 70
5007 Bergen, Norway
T. +47 55 23 66 00

Tromsø
P.O. Box 6314,
Langnes
9293 Tromsø, Norway
T. +47 77 62 13 00

www.met.no

(see Fig. 3), which means that the southern tip is more often surrounded by open water in the MPI-ESM-based simulation than in CARRA. In contrast, there are some areas in the north, where the model overestimates the number of frost days, so sea ice can not explain all of the difference.

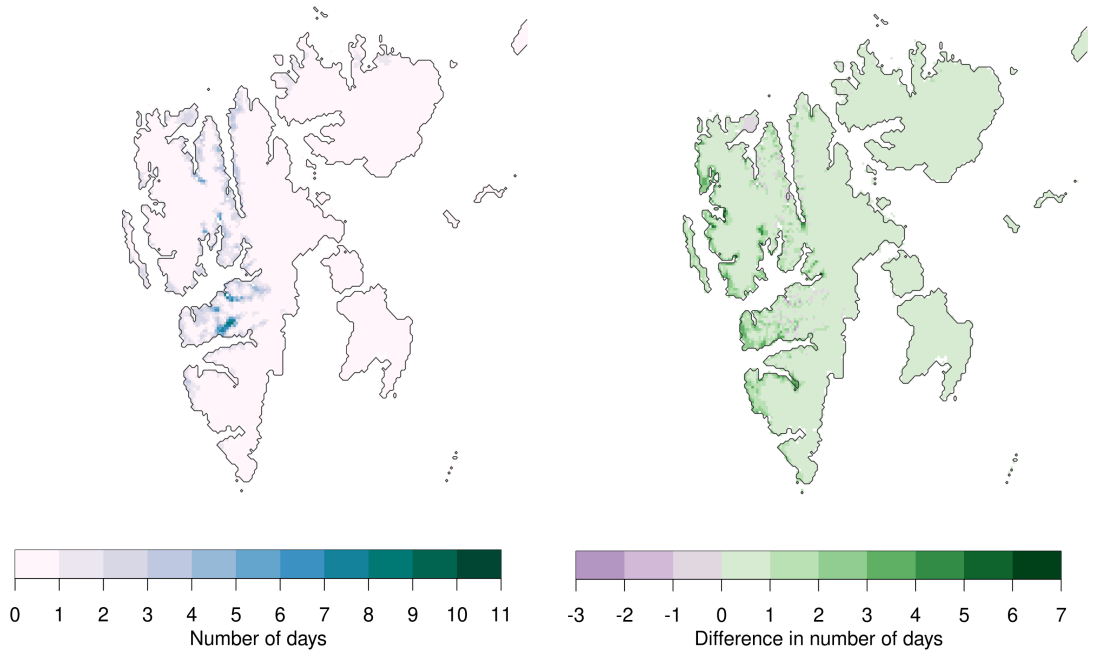

Figure 6 *Left*: Mean annual number of days with daily mean temperature > 10 °C for 1991–2020, derived from CARRA. *Right*: Difference in the mean annual number of days with T_{mean} > 10 °C between HCLIM43-AROME (driven by MPI-ESM1-2-LR) and CARRA.

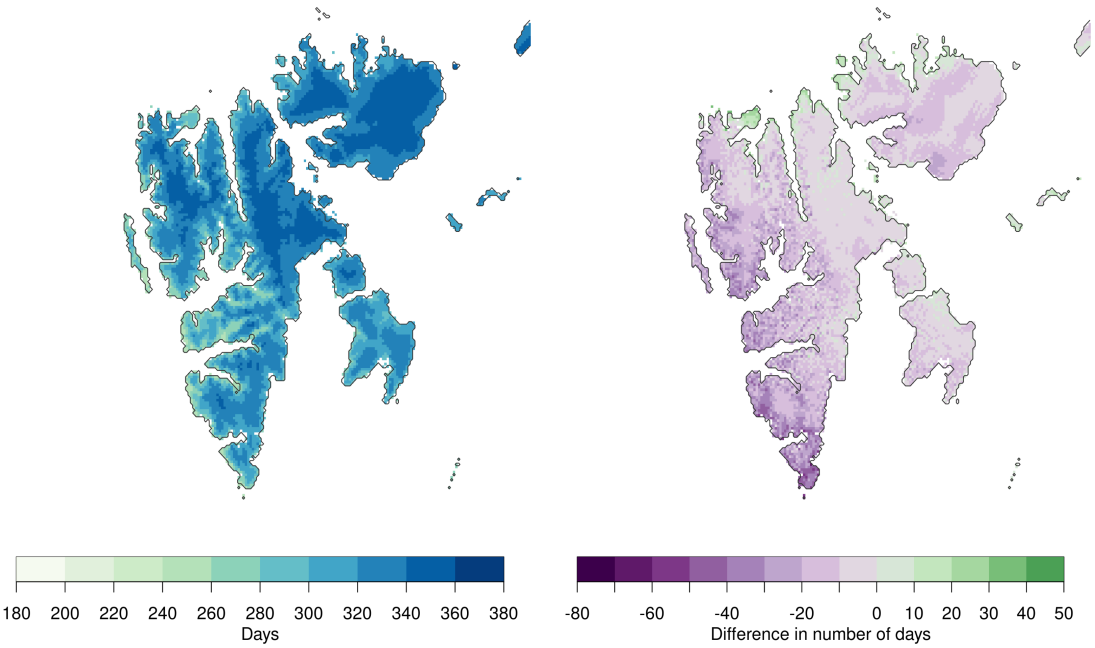

Figure 7 *Left*: Mean annual number of days with daily minimum temperature < 0 °C for 1991–2020, derived from CARRA. *Right*: Difference in the mean annual number of days with T_{min} < 0 °C between HCLIM43-AROME (driven by MPI-ESM1-2-LR) and CARRA.

The left panel of Figure 8 illustrates the mean annual number of zero crossing days for the period 1991–2020, derived from CARRA data. Also referred to as frost-change days, zero crossing days are defined as days when the minimum temperature drops below 0 °C while the maximum temperature rises above 0 °C. These days are most frequent in southern and coastal areas of Svalbard, while the fewest occurrences are located in the colder, glaciated inland areas of the north and northeast. The right panel of Figure 8 shows the difference between the MPI-ESM-based simulation and the CARRA dataset. The discrepancies vary across Svalbard: while the model tends to underestimate the number of zero crossing days in some areas, particularly along the coasts of Nordaustlandet, northern Spitsbergen, and around Isfjorden, it generally overestimates them elsewhere. The overestimation is most pronounced in southeastern Spitsbergen, on Prins Karls Forland and at Velkomstpynten, where the difference can reach up to 30 days. Again, this may be indicative of days with ice-free conditions in the winter, as the open ocean easily warms surrounding air to temperatures closer to 0 °C.

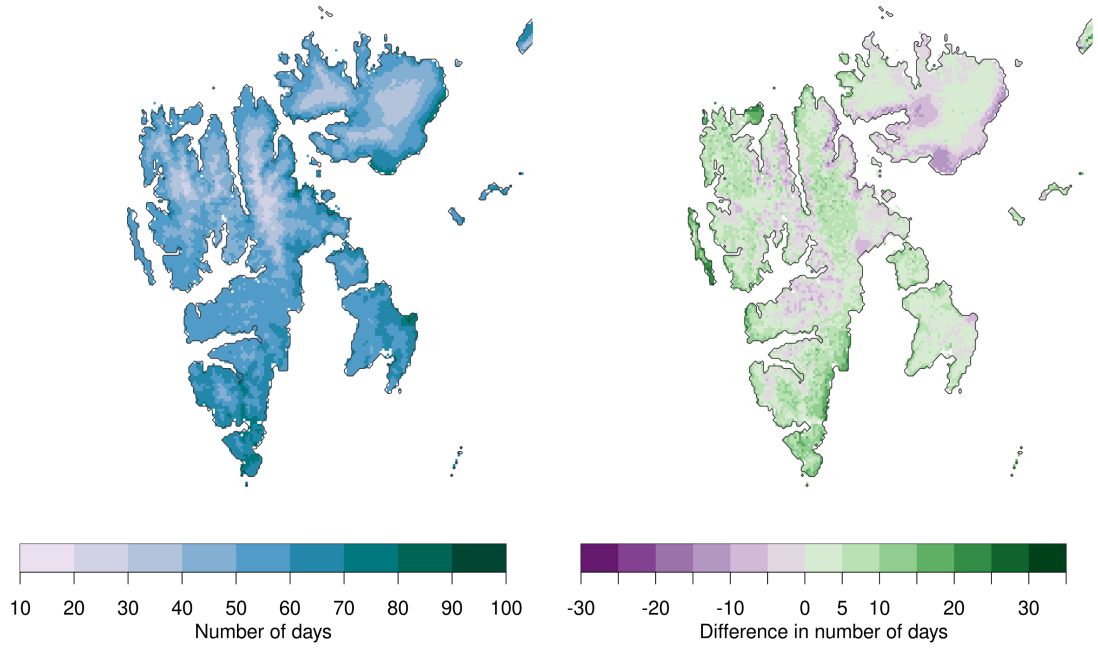

Figure 8 *Left*: Mean annual number of zero crossing days (T_{min} < 0 °C & T_{max} > 0 °C) for 1991–2020, derived from CARRA. *Right*: Difference in the mean annual number of zero crossing days between HCLIM43-AROME (driven by MPI-ESM1-2-LR) and CARRA.

Climate indices derived from precipitation

Figure 9 illustrates the mean annual number of wet days derived from CARRA for 1991–2020 and the difference between the MPI-ESM-based simulation and CARRA. Wet days are defined as days with at least 1 mm of precipitation (for snow, graupel or hail, this refers to the liquid water equivalent). In CARRA, most wet days are concentrated in the southern parts of Spitsbergen. The simulation manages quite well to capture the pattern in the number of wet

Meteorologisk institutt
Meteorological Institute
Org.no 971274042
post@met.no

Oslo
P.O. Box 43 Blindern
0313 Oslo, Norway
T. +47 22 96 30 00

Bergen
Allégaten 70
5007 Bergen, Norway
T. +47 55 23 66 00

Tromsø
P.O. Box 6314,
Langnes
9293 Tromsø, Norway
T. +47 77 62 13 00

www.met.no

days, with Edgeøya, Barentsøya and the southeastern tip of Spitsbergen having a slight overestimation compared to CARRA.

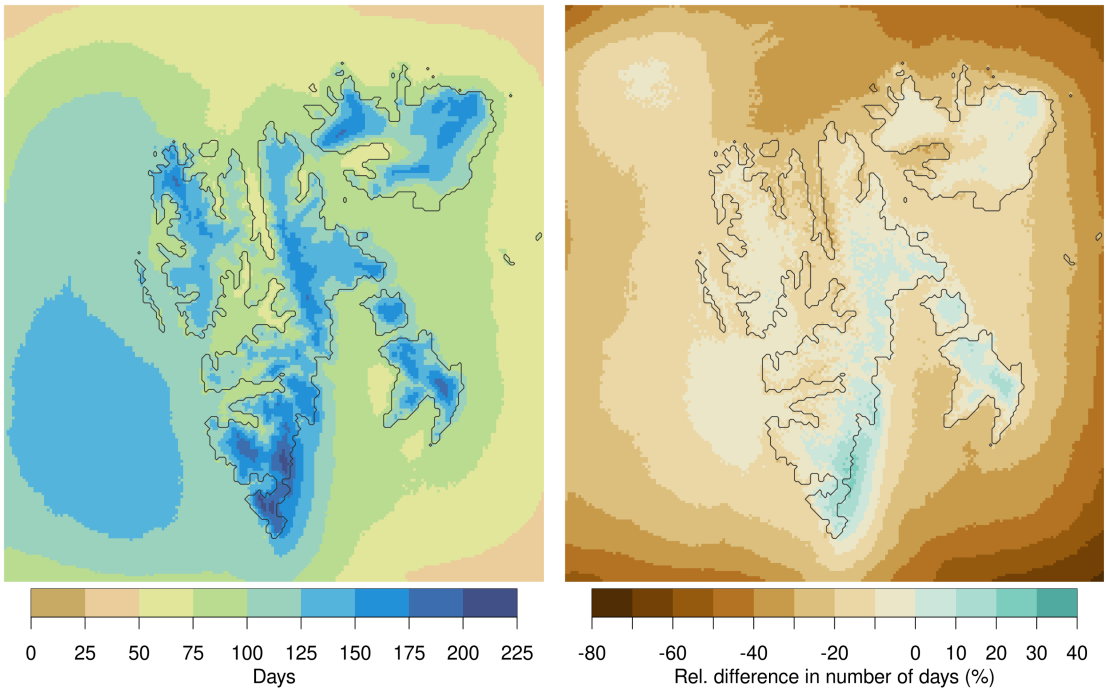

Figure 9 *Left*: Mean annual number of wet days (≥ 1 mm of precipitation) for 1991–2020, derived from CARRA. *Right*: Relative difference in the mean annual number of wet days between HCLIM43-AROME (driven by MPI-ESM1-2-LR) and CARRA.

The left panel of Figure 10 shows the mean annual precipitation amount on wet days for 1991–2020, based on CARRA. The right panel displays the difference between the simulation based on MPI-ESM and CARRA for the same period. In CARRA, the highest precipitation amounts of around 10 mm/day occur primarily in southeastern Spitsbergen, with notable high values also found in northwestern Spitsbergen and southern Edgeøya. Comparing the left panels of Figures 9 and 10 reveals that while wet days are frequent across Svalbard, precipitation intensity remains relatively low. The difference between the MPI-ESM simulation and CARRA indicates that the HCLIM43 simulation based on MPI-ESM generally yields higher precipitation intensities, particularly over land, with the largest differences, 30-40 %, occurring in northern Spitsbergen.

The number of very heavy precipitation days, defined as days with at least 20 mm of daily precipitation, is presented in Figure 11. As in previous figures, the left panel shows CARRA data for 1991–2020, while the right panel displays the difference between the MPI-ESM-based simulation and CARRA. As stated in the section before, the precipitation intensity on Svalbard is generally low. Thus, the number of very heavy precipitation days in CARRA is very low as well, ranging from approximately 5 to 20 days in the wettest areas of Svalbard. Overall, the HCLIM43 simulation based on MPI-ESM overestimates the number of these days, particularly in the southeast of Spitsbergen, where the difference can exceed 10 days.

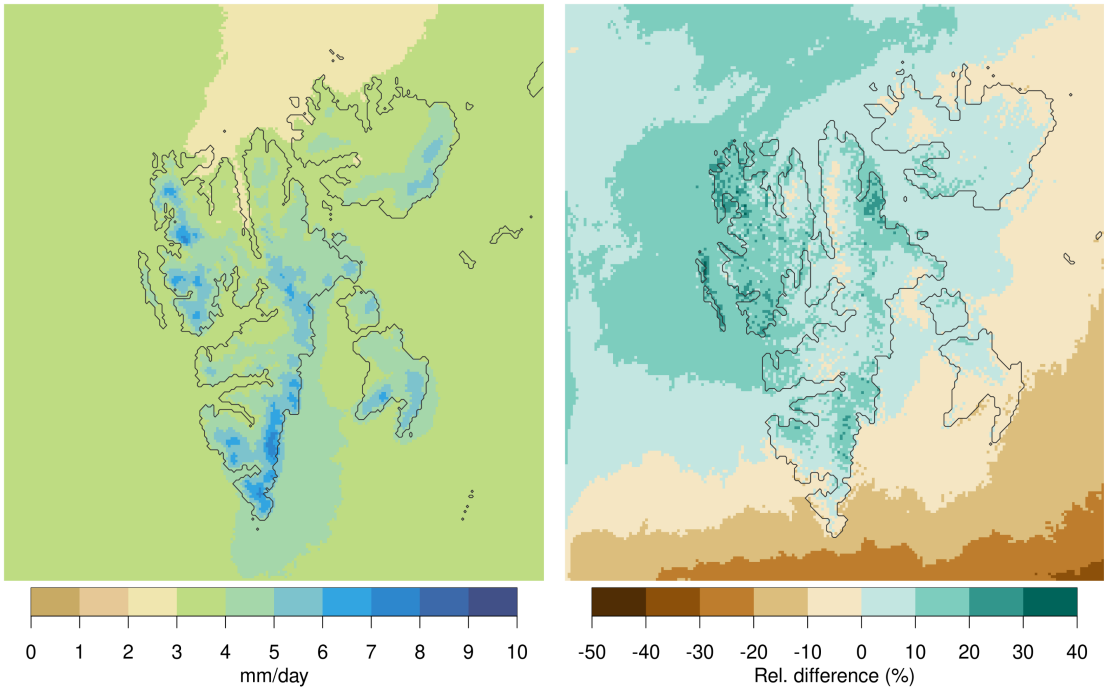

Figure 10 *Left*: Mean annual precipitation amount on wet days for 1991–2020, derived from CARRA. *Right*: Relative difference in the mean annual precipitation amount on wet days between HCLIM43-AROME (driven by MPI-ESM1-2-LR) and CARRA.

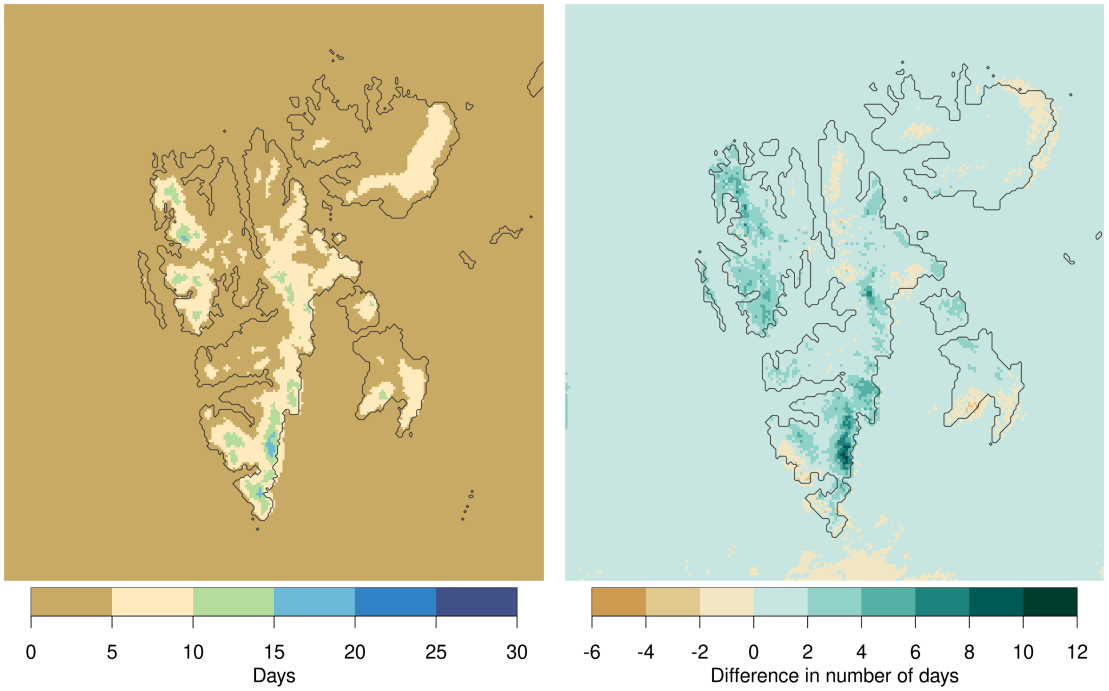

Figure 11 *Left*: Mean annual number of very heavy precipitation days (≥ 20 mm of precipitation) for 1991–2020, derived from CARRA. *Right*: Relative difference in the mean annual number of very heavy precipitation days between HCLIM43-AROME (driven by MPI-ESM1-2-LR) and CARRA.

Meteorologisk institutt
Meteorological Institute
Org.no 971274042
post@met.no

Oslo
P.O. Box 43 Blindern
0313 Oslo, Norway
T. +47 22 96 30 00

Bergen
Allégaten 70
5007 Bergen, Norway
T. +47 55 23 66 00

Tromsø
P.O. Box 6314,
Langnes
9293 Tromsø, Norway
T. +47 77 62 13 00

www.met.no

3.2 Climate change projections for Svalbard

The main purpose of the simulations are to allow for an assessment of possible future climate change in Svalbard following the high emissions scenario SSP5-8.5. The mean changes in annual and seasonal temperature and precipitation between the reference period (1991–2020) and 2041–2070 are shown in Fig. 12. The simulation projects a general temperature increase of approximately 3.2 °C for the whole simulation area. The annual precipitation is projected to increase as well, especially over land. The mean precipitation change is approximately 6 % for the whole simulation domain.

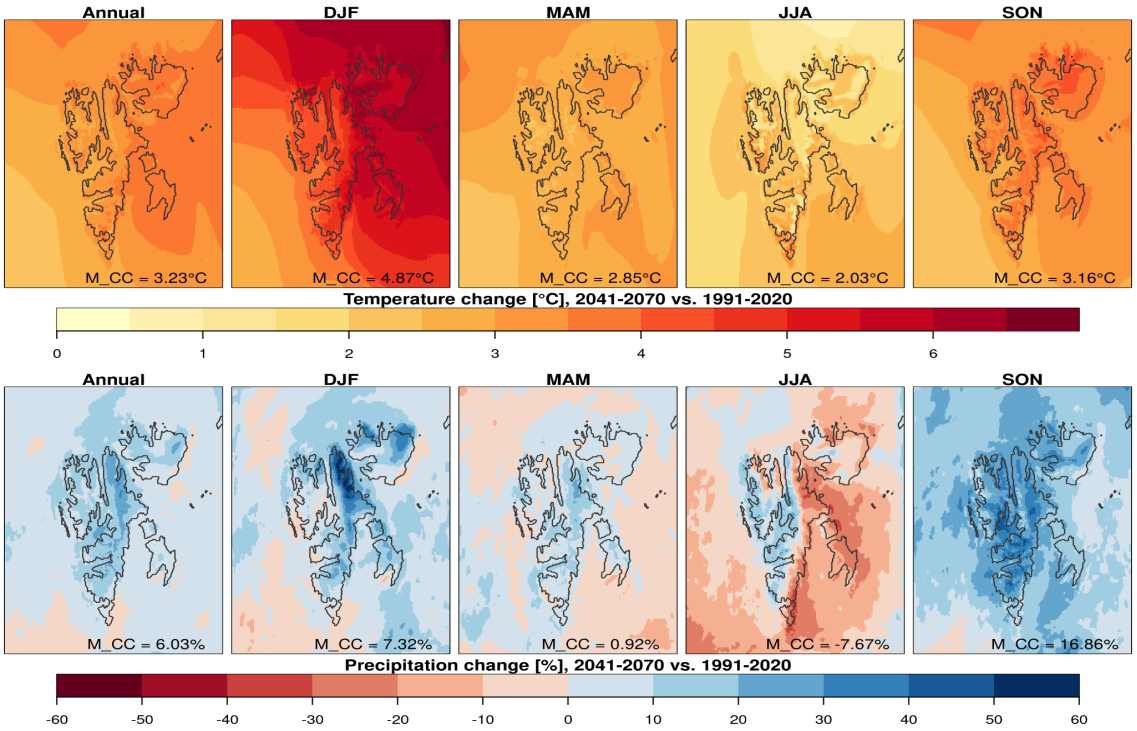

Figure 12 Change in 2-metre temperature (top) and precipitation (bottom) from 1991–2020 to 2041–2070, following the SSP5-8.5 scenario in the HCLIM43-AROME simulation based on MPI-ESM .

Comparing seasonal changes between 2041–2070 and 1991–2020, the simulation indicates the strongest warming (approx. 4.9 °C) during winter, with a pronounced east-west gradient. This warming is linked to sea ice retreat, as northeastern areas transition from being predominantly ice-covered in the reference period to more ice-free conditions in the future. A similar, albeit weaker, gradient is projected in autumn. In contrast, summer experiences the weakest warming (approx. 2 °C), with localised hotspots along the western and southern coasts.

For precipitation (Fig. 12, lower panels), the simulations project the strongest increase (approx. 17 %) in autumn, affecting the entire archipelago. In winter, a significant rise is expected east of Wijdefjorden (Ny-Friesland). Summer, however, reveals a notable contrast between the west and east: western regions are projected to become wetter (except along the northern coast), while eastern areas may experience drier conditions, possibly reflecting shifts in atmospheric circulation patterns.

When comparing this simulation run with the climate projections in the *Climate in Svalbard 2100* report (Hanssen-Bauer et al., 2019), we see a similar general spatial pattern. In both cases,

winter emerges as the season with the largest temperature increase. However, the changes between past and future climate are based on different timeframes: this study examines periods 50 years apart (2041–2070 vs. 1991–2020), whereas the time periods in Hanssen-Bauer et al. (2019) are 100 years apart (2071–2100 vs. 1971–2000). As a result, their projected temperature increases are significantly higher. The differences in projected precipitation are even more pronounced. Nonetheless, Hanssen-Bauer et al. (2019) also report a substantial increase in winter precipitation in northeastern Svalbard. These differences between temperature and precipitation align with the general understanding that temperature projections tend to be more robust and hence more consistent across models, while precipitation projections are inherently more uncertain and variable.

Climate indices derived from temperature

The simulated average number of growing days (daily mean temperature > 5 °C) is very low across most of Svalbard in the reference period, as much of the archipelago remains glacier-covered and experiences none. The highest values, ranging from one to three months, occur along the western coast of Spitsbergen, including the fjords (Fig. 13, left). Projections for 2041–2070 under the strong warming scenario SSP5-8.5 (Fig. 13, right) suggest a considerable increase in growing days in southern coastal areas, while northeastern inland regions will continue to have very few, even under this high-emission scenario. These findings align well with the *Climate in Svalbard 2100* report (Hanssen-Bauer et al., 2019). For the southern coastal areas the changes correspond to a growing season of three to four months.

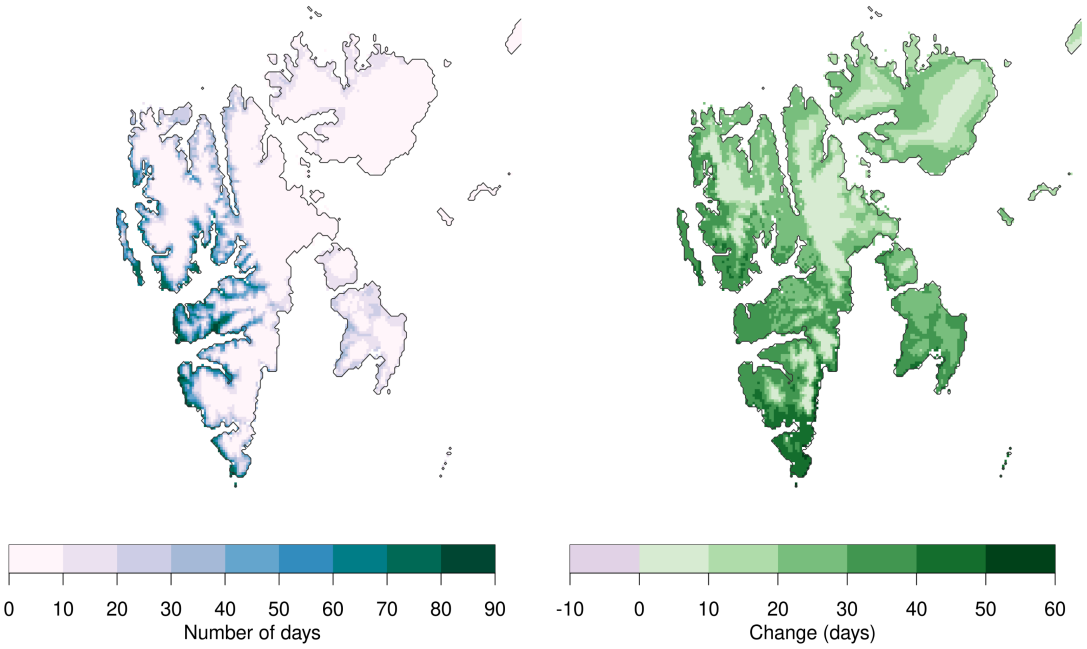

Figure 13 Average number of days with daily mean temperature > 5 °C per year for the period 1991–2020 (*left*). Changes from 1991–2020 to 2041–2070 under a high emission scenario (SSP5-8.5) for the average number of these days (*right*). Numbers are based on simulations from HCLIM43-AROME (driven by MPI-ESM1-2-LR).

Meteorologisk institutt
Meteorological Institute
Org.no 971274042
post@met.no

Oslo
P.O. Box 43 Blindern
0313 Oslo, Norway
T. +47 22 96 30 00

Bergen
Allégaten 70
5007 Bergen, Norway
T. +47 55 23 66 00

Tromsø
P.O. Box 6314,
Langnes
9293 Tromsø, Norway
T. +47 77 62 13 00

www.met.no

As expected, the simulated average number of warm days (daily mean temperature > 10 °C) during the reference period is even lower than the number of growing days. The highest values, ranging from four to eleven days, are concentrated along the western coast of Spitsbergen, especially around Isfjorden and Van Mijenfjorden (Fig. 14, left). Projections for 2041–2070 under SSP5-8.5 (Fig. 14, right) indicate a considerable increase in warm days in these areas. However, northeastern inland regions are expected to remain largely unaffected, with very few warm days even under this high-emission scenario.

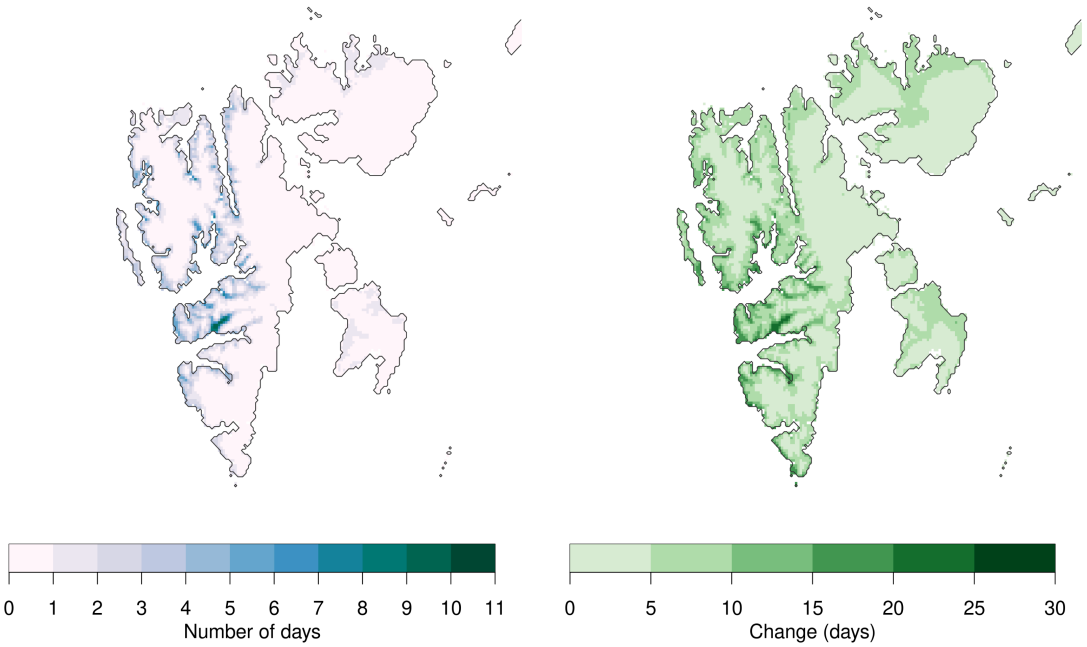

Figure 14 Average number of days with daily mean temperature > 10 °C per year for the period 1991–2020 (*left*). Changes from 1991–2020 to 2041–2070 under a high emission scenario (SSP5-8.5) for the average number of these days (*right*). Numbers are based on simulations from HCLIM43-AROME (driven by MPI-ESM1-2-LR).

In the MPI-ESM-based simulation, the average number of frost days (daily minimum temperature < 0 °C) on Svalbard for the period 1991–2020 is approximately 310 per year. The highest values occur in the northern and northeastern glacial regions (see Figure 15, left panel), while the lowest can be found along the west coast of Spitsbergen. Projections for 2041–2070 indicate a considerable decrease in frost days for the southeastern coastal areas and on Edgeøya, whereas the reduction remains limited in the northern and northeastern inland areas (Figure 15, right panel).

The left panel of Figure 16 presents the simulated mean annual number of zero crossing days for the period 1991–2020. On average, the model simulates approximately 55 such days per year on Svalbard. The highest values occur in the south and along the coasts, with values of 70 to 100 days per year. Projected changes in the annual number of zero crossing days indicate a general increase across the archipelago (Fig. 16, right panel). The largest increases are projected in the colder regions, particularly in Nordaustlandet, while only minor changes are expected along the west coast of Spitsbergen. These results are consistent with the findings reported in *Climate in Svalbard 2100* (Hanssen-Bauer et al., 2019).

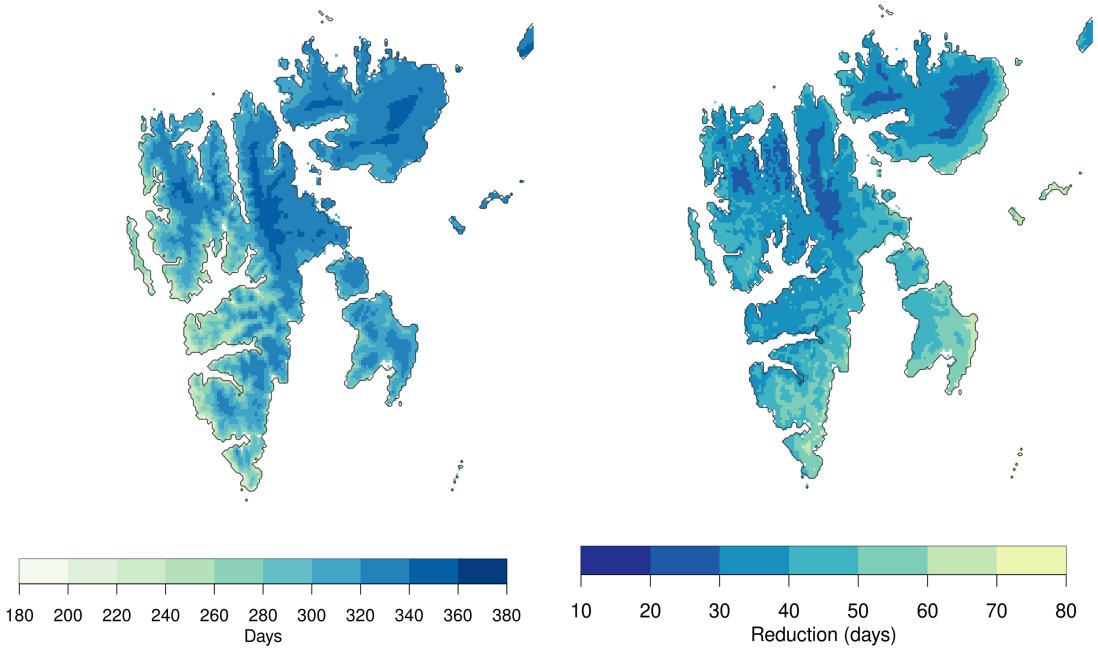

Figure 15 Mean annual number of frost days (daily minimum temperature < 0 °C) for 1991–2020 (*left*). Reduction in the number of frost days from 1991–2020 to 2041–2070 under a high emission scenario (SSP5-8.5) (*right*). Numbers are based on simulations from HCLIM43-AROME (driven by MPI-ESM1-2-LR).

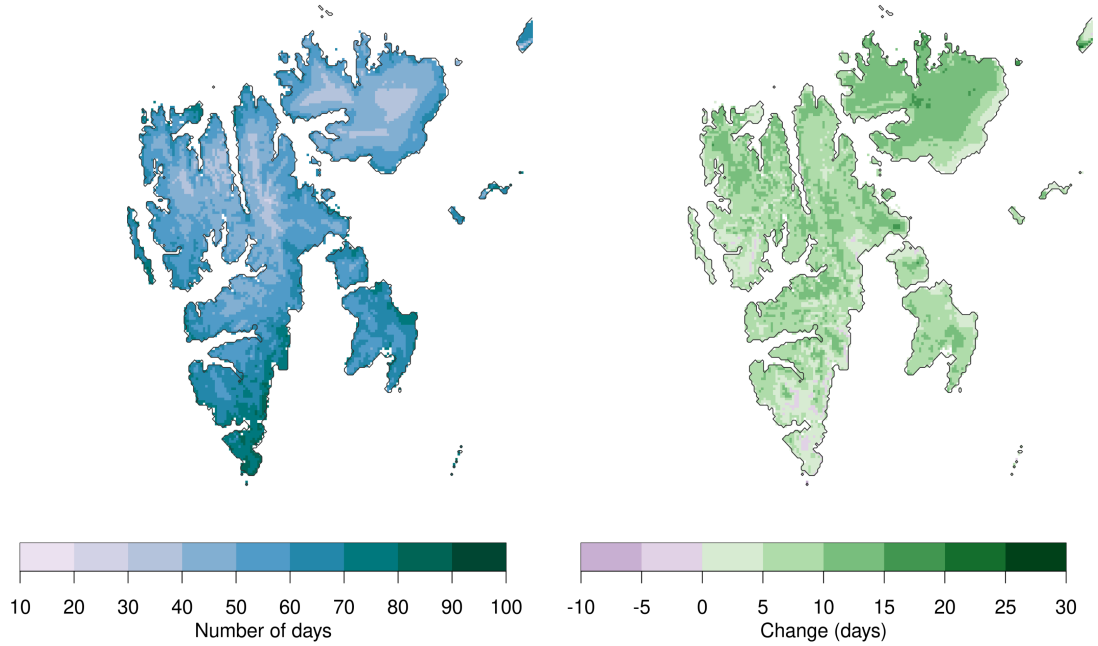

Figure 16 Mean annual number of zero crossing days (T_{min} < 0 °C & T_{max} > 0 °C) for 1991–2020 (*left*). Change in the number of zero crossing days from 1991–2020 to 2041–2070 under a high emission scenario (SSP5-8.5) (*right*). Numbers are based on simulations from HCLIM43-AROME (driven by MPI-ESM1-2-LR).

Meteorologisk institutt
Meteorological Institute
Org.no 971274042
post@met.no

Oslo
P.O. Box 43 Blindern
0313 Oslo, Norway
T. +47 22 96 30 00

Bergen
Allégaten 70
5007 Bergen, Norway
T. +47 55 23 66 00

Tromsø
P.O. Box 6314,
Langnes
9293 Tromsø, Norway
T. +47 77 62 13 00

www.met.no

Climate indices derived from precipitation

The simulated average number of wet days (defined as days with at least 1 mm of precipitation) is relatively high across most of Svalbard during the reference period. The highest values, ranging from 200 to 225 days per year, occur in the south of Spitsbergen (Fig. 17, left panel). However, the simulated average precipitation amount on these days is relatively low (Fig. 17, right panel). The highest daily precipitation totals on wet days, ranging from 7 to 10 mm, can be found in the southeast and northwest of Spitsbergen, while most other areas receive only 3-5 mm on average. This pattern of many wet days but low precipitation amounts on these days agrees well with the CARRA data (see Section 3.1).

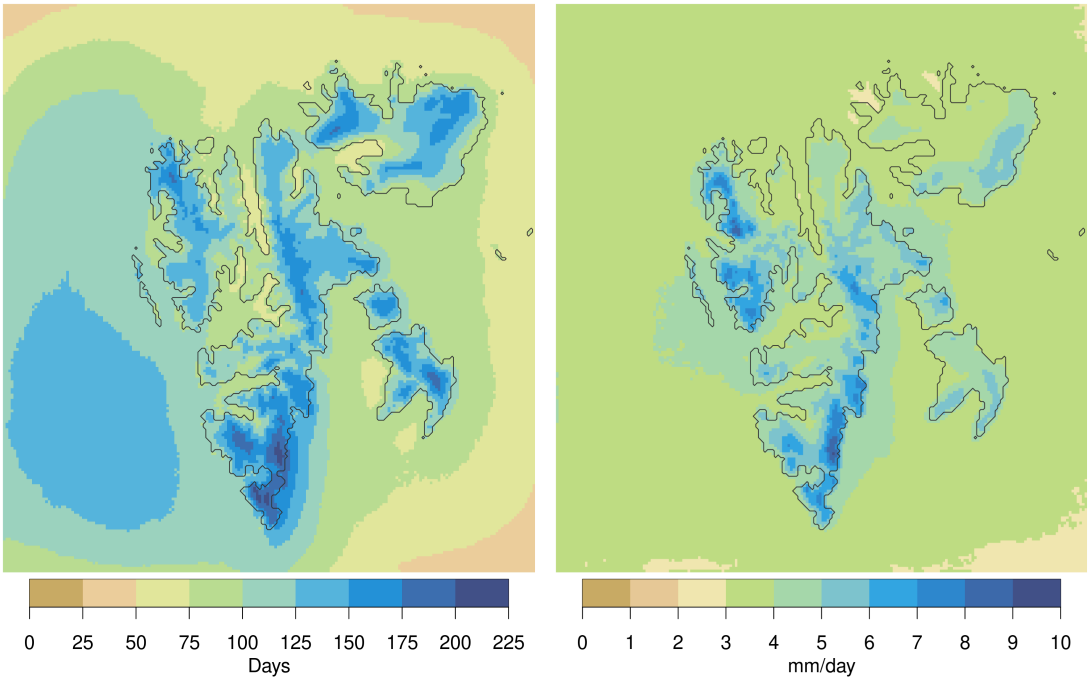

Figure 17 Average number of wet days (≥ 1 mm of precipitation) per year (*left*) and mean precipitation amount on these days (*right*) for the period 1991–2020, based on model data from HCLIM43-AROME (driven by MPI-ESM1-2-LR).

Projections for 2041–2070 under the SSP5-8.5 scenario indicate a slight increase in the number of wet days over Svalbard, especially in the northwest (Fig. 18, left panel), with the largest increases reaching 10-12 additional wet days per year. Precipitation intensity, defined as the amount of precipitation on wet days, is also projected to increase across nearly the entire area of interest (Fig. 18, right panel). The most pronounced changes, with increases between 10 % and 20 %, are expected in central and northeastern Spitsbergen. These combined changes indicate that, in the future, not only will wet days become more frequent, but they will also bring more precipitation when they occur.

Figure 19 presents the average number of very heavy precipitation days (daily precipitation > 20 mm) on Svalbard during the period 1991–2020, based on the MPI-ESM simulation. Given Svalbard's current climate, where such extreme precipitation events are rare, the overall number of such days is low as well. The highest values, ranging from 15 to 30 days per year, occur in the southeast of Spitsbergen (Figure 19, left panel), while the lowest can be found over the ocean and Nordaustlandet. Projections for 2041–2070 indicate a slight increase in very heavy

precipitation days for eastern Spitsbergen, where the model estimates additional 2 to 4 such days annually (Figure 19, right panel).

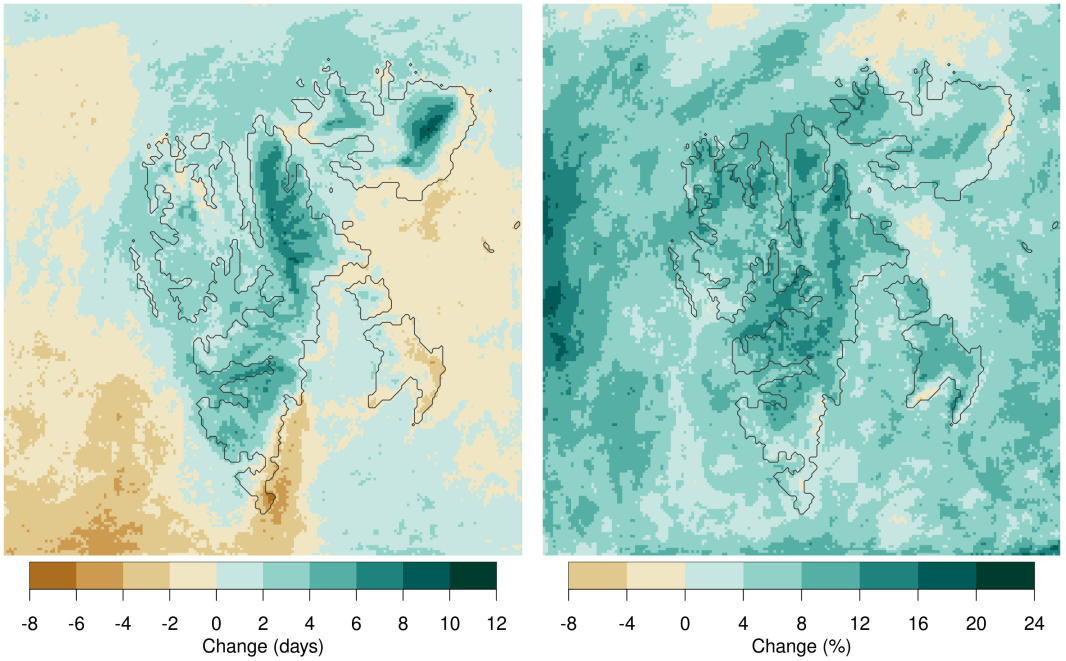

Figure 18 Changes from 1991–2020 to 2041–2070 under a high emission scenario (SSP5-8.5) for the average number of wet days per year (*left*) and the mean precipitation amount on these days (*right*), based on simulations from HCLIM43-AROME (driven by MPI-ESM1-2-LR).

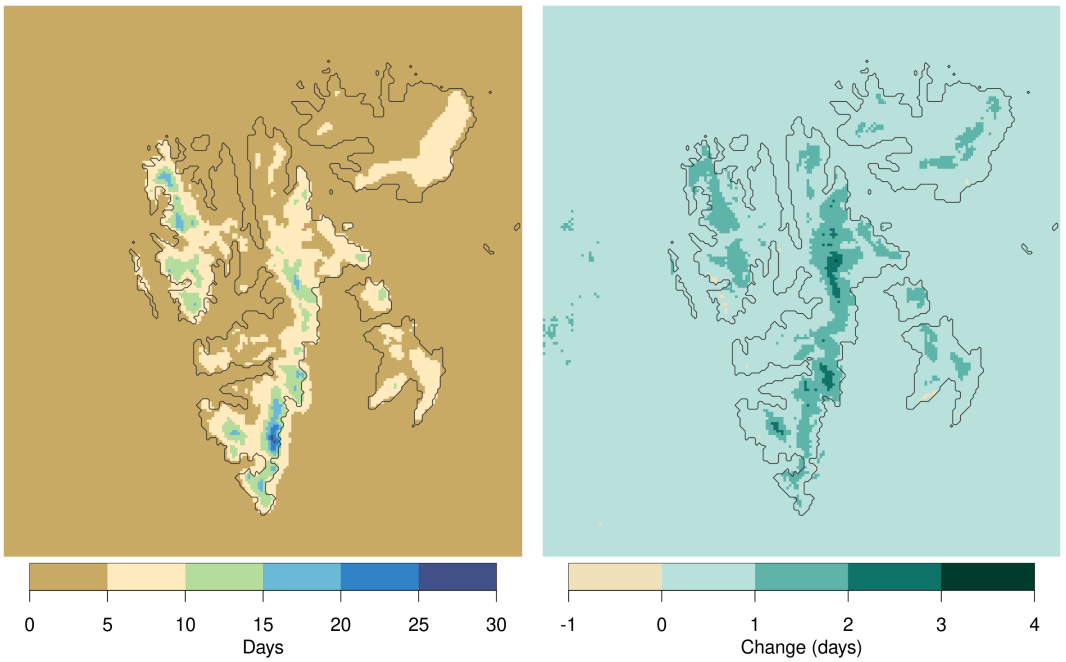

Figure 19 Average number of days with precipitation amounts of at least 20 mm for the period 1991–2020 (*left*). Changes from 1991–2020 to 2041–2070 under a high emission scenario (SSP5-8.5) for the average number of these days (*right*). Numbers are based on simulations from HCLIM43-AROME (driven by MPI-ESM1-2-LR).

Meteorologisk institutt
Meteorological Institute
Org.no 971274042
post@met.no

Oslo
P.O. Box 43 Blindern
0313 Oslo, Norway
T. +47 22 96 30 00

Bergen
Allégaten 70
5007 Bergen, Norway
T. +47 55 23 66 00

Tromsø
P.O. Box 6314,
Langnes
9293 Tromsø, Norway
T. +47 77 62 13 00

www.met.no

The left panel of Figure 20 illustrates the fraction of autumn precipitation (September to November) falling as snow, based on the MPI-ESM-driven simulation. In western Spitsbergen, around 50 % of the precipitation falls as snow, whereas in the east, particularly the glaciated areas of the northeast, this fraction is significantly higher, ranging from 80 % to 100 %. For the period 2041–2071, a notable decrease in the snow fraction is projected for the southwestern coastal areas. Nonetheless, glaciated regions such as Ny-Friesland, Olav V Land, and Nordaustlandet are expected to continue receiving the majority of their autumn precipitation as snow, even under future climate conditions.

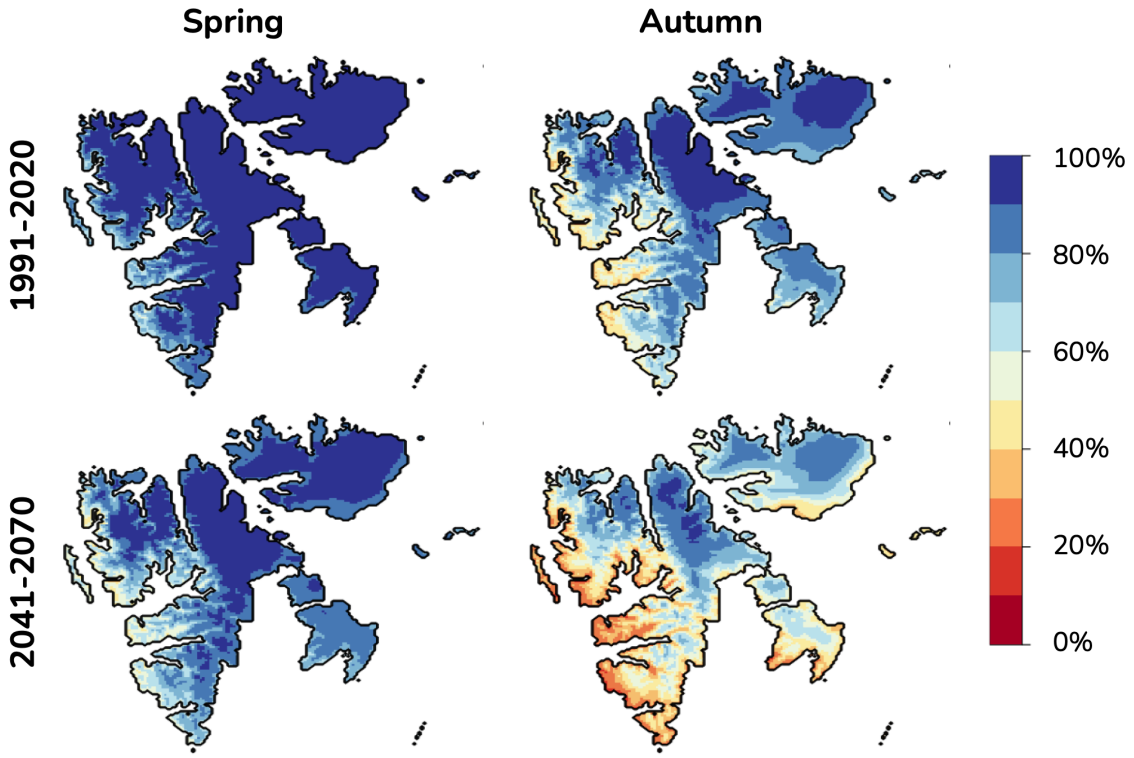

Figure 20 Fraction of spring (Mar-May, left) and autumn (Sep-Nov, right) precipitation falling as snow for the two time periods 1991–2020 (top) and 2041–2070 (bottom).

3.3 Impacts in Longyearbyen and Ny-Ålesund

The projected temperature changes in the two study areas are summarised in Table 1. Both annual and seasonal temperature changes are very similar across the two areas. Compared to the 1991–2020 period, the daily mean temperature is projected to increase by 1.8 °C in Longyearbyen/Adventdalen and 1.9 °C in Ny-Ålesund for the period 2021–2050. This increase becomes more pronounced for 2041–2070, with a projected rise of 3.3 °C in both areas in HCLIM43-AROME based on MPI-ESM1-2-LR in the SSP5-8.5 scenario.

The strongest increase in daily mean temperature, in both areas, is projected for the winter season, with temperatures rising by 4.5 °C in Longyearbyen/Adventdalen and 4.4 °C in Ny-Ålesund by 2041–2070 relative to 1991–2020. This increase is approximately double that of the summer season, where temperatures are projected to rise by 2.1 °C and 2.2 °C in Longyearbyen/Adventdalen and Ny-Ålesund, respectively.

For daily minimum temperature, the strongest increase between 1991–2020 and 2041–2070 is also simulated in winter, reaching 4.1 °C in Longyearbyen/Adventdalen and 3.9 °C in Ny-Ålesund. In contrast, the weakest change in minimum temperature is projected for summer, with values of 2.0 °C and 2.1 °C, respectively. The same pattern is projected for daily maximum temperature, although the difference between the strongest and weakest seasonal increases are smaller. Maximum temperatures are simulated to rise by 3.7 °C in Longyearbyen/Adventdalen and 3.4 °C in Ny-Ålesund during winter, while summer increases are expected to be 2.1 °C and 2.2 °C, respectively.

Table 1 Change in temperature (increase in °C relative to 1991–2020) averaged over the selected grid cells representative of Longyearbyen+Adventdalen and Ny-Ålesund from the 2.5 km simulation downscaled with HCLIM-AROME from MPI-ESM1-2-LR following the SSP5-8.5 scenario. The daily mean, minimum and maximum 2-metre temperature are given in columns, separated into annual, winter (Dec-Feb), spring (Mar-May), summer (Jul-Aug) and autumn (Sep-Nov) seasons, respectively.

	Daily mean temperature (tas) change [°C]					Daily minimum temperature (tasmin) change [°C]					Daily maximum temperature (tasmax) change [°C]				
Time period	**ANN**	**DJF**	**MAM**	**JJA**	**SON**	**ANN**	**DJF**	**MAM**	**JJA**	**SON**	**ANN**	**DJF**	**MAM**	**JJA**	**SON**
Longyearbyen and Adventdalen															
2021–2050	1.8	2.2	1.8	1.1	2.3	1.7	2.0	1.5	1.1	2.1	1.6	1.9	1.5	1.2	1.9
2041–2070	3.3	4.5	3.1	2.1	3.4	3.0	4.1	2.6	2.0	3.1	2.8	3.7	2.5	2.1	2.8
Ny-Ålesund															
2021–2050	1.9	2.1	2.1	1.3	2.2	1.8	1.9	1.8	1.3	2.0	1.6	1.7	1.6	1.4	1.8
2041–2070	3.3	4.4	3.3	2.2	3.3	2.9	3.9	2.8	2.1	3.0	2.7	3.4	2.5	2.2	2.8

Table 2 presents the projected relative changes in total precipitation for both study areas, along with the fraction of total precipitation falling as snow. Unlike temperature, precipitation changes exhibit larger differences between the two study areas. Despite these differences, the simulations indicate an overall increase in annual total precipitation for both areas.

Compared to the 1991–2020 period, total annual precipitation is projected to increase by 16 % in Longyearbyen/Adventdalen and 10 % in Ny-Ålesund for 2021–2050. This increase becomes more pronounced for the 2041–2070 period, reaching 23 % in Longyearbyen/Adventdalen and 14 % in Ny-Ålesund.

The strongest seasonal increase in total precipitation, in both areas, is projected for autumn, with precipitation rising by 40 % in Longyearbyen/Adventdalen and 17 % in Ny-Ålesund by 2041–2070 relative to 1991–2020. Notably, the seasonal distribution of precipitation change differs significantly between the two areas. In Longyearbyean/Adventdalen, the autumn increase

Meteorologisk institutt
Meteorological Institute
Org.no 971274042
post@met.no

Oslo
P.O. Box 43 Blindern
0313 Oslo, Norway
T. +47 22 96 30 00

Bergen
Allégaten 70
5007 Bergen, Norway
T. +47 55 23 66 00

Tromsø
P.O. Box 6314,
Langnes
9293 Tromsø, Norway
T. +47 77 62 13 00

www.met.no

is twice as large as the next-highest seasonal increase in winter (20 %) and more than three times the weakest increase in spring (12 %). In contrast, seasonal changes in Ny-Ålesund are more balanced, with the weakest projected precipitation increases occurring in summer and winter, both at 12 %.

The right side of Table 2 illustrates projected changes in the fraction of total precipitation falling as snow in both study areas. Across all seasons, the snow fraction is projected to decline, with very similar trends in both areas. In Longyearbyen/Adventdalen, the annual snow fraction for the reference period (1991–2020) is 51 %. This is projected to decrease to 43 % in 2021–2050, and further to 37 % in 2041–2070. In Ny-Ålesund, the initial value is already lower at 45 %, dropping to 38 % in 2021–2050 and then to 32 % in 2041–2070.

Table 2 Change in precipitation (relative to 1991–2020) averaged over the selected grid cells representative of Longyearbyen+Adventdalen and Ny-Ålesund from the 2.5 km simulation downscaled with HCLIM-AROME from MPI-ESM1-2-LR following the SSP5-8.5 scenario. The change in annual mean as well as the different seasons are given in separate columns.

	Change in total precipitation (rain+snow+graupel) [% relative to 1991–2020]					**Fraction of precipitation falling as snow** [% of total precipitation]				
Time period	**ANN**	**DJF**	**MAM**	**JJA**	**SON**	**ANN**	**DJF**	**MAM**	**JJA**	**SON**
Longyearbyen and Adventdalen										
2021–2050	+16%	+22%	-6%	+13%	+27%	43%	71%	67%	2%	33%
2041–2070	+23%	+20%	+12%	+14%	+40%	37%	64%	56%	0%	27%
Ny-Ålesund										
2021–2050	+10%	+17%	-4%	+6%	+16%	38%	64%	54%	3%	29%
2041–2070	+14%	+12%	+15%	+12%	+17%	32%	56%	44%	2%	24%

Seasonal changes vary in magnitude. In Longyearbyen/Adventdalen, the largest reduction between 1991–2020 and 2021–2050 occurs in autumn (13 %), while in Ny-Ålesund, spring experiences the highest decline in snow fraction (11 %). Summer shows the smallest reductions: 4 % in Longyearbyen/Adventdalen and 3 % in Ny-Ålesund.

The strongest seasonal decrease in snow fraction between the two future periods is projected for spring, with reductions of 11 % in Longyearbyen/Adventdalen and 10 % in Ny-Ålesund. In contrast, the weakest decrease is projected for the summer season, with declines of just 2 % and 1 %, respectively.

4 Summary

In this report, we employed the HARMONIE-Climate (HCLIM) regional climate model to dynamically downscale climate projections over Svalbard, using input from two CMIP6 global models, MPI-ESM1-2-LR and NorESM2-MM, under the high-emission scenario SSP5-8.5. These models represent contrasting Arctic climate futures, with differences in regional warming patterns and sea ice representation. Due to the coarse resolution of the global models, a nested approach was used: a 12 km resolution outer domain and a 2.5 km inner domain centered on Svalbard. Additionally, we carried out an evaluation simulation, based on ERA5 data, to help assess the model performance. All simulations were compared against the Copernicus Arctic Regional Reanalysis (CARRA) data, either for the 1991–2020 reference period or for 2000–2020 in the case of ERA5.

Our results show that the downscaled ERA5 simulation closely resembles CARRA in terms of temperature and precipitation, while simulations driven by the global models display regional biases, some of which can be explained by their difference in sea ice concentrations. The MPI-ESM-based simulation aligns more closely with CARRA than the one based on NorESM, especially regarding temperature and sea ice distribution, making it the preferred basis for future projections. This simulation allows for a fine-scale representation of climate change impacts under the high emissions scenario SSP5-8.5. However, users should interpret results cautiously, as conclusions drawn from a limited number of simulations may not capture the full range of possible futures. We therefore encourage supplementing these results with additional simulations, such as those from the Arctic CORDEX initiative, which offer longer time periods at coarser resolution, or by applying complementary methods like empirical-statistical downscaling performed directly to global CMIP outputs.

We further evaluated the MPI-ESM-based HCLIM simulation for a set of climate indices of particular relevance to human activities and ecology. Key climate indices derived from temperature—such as growing days, warm days, frost days, and zero crossing days—demonstrate that the model captures spatial patterns well, though it tends to overestimate growing and warm days while underestimating frost days. Precipitation-related indices indicate that the model reproduces the frequency and intensity of wet days reasonably, although it tends to over-represent very heavy precipitation events, especially in southeastern Spitsbergen.

Looking ahead to 2041–2070, simulations project significant warming (around 3.2 °C in annual mean compared to 1991-2020) and moderate increases in precipitation (about 6 % overall), with the strongest temperature rise in winter (around 4.9 °C) linked to sea ice retreat. The number of

Meteorologisk institutt
Meteorological Institute
Org.no 971274042
post@met.no

Oslo
P.O. Box 43 Blindern
0313 Oslo, Norway
T. +47 22 96 30 00

Bergen
Allégaten 70
5007 Bergen, Norway
T. +47 55 23 66 00

Tromsø
P.O. Box 6314,
Langnes
9293 Tromsø, Norway
T. +47 77 62 13 00

www.met.no

growing and warm days is expected to rise, especially in coastal regions, while frost days are projected to decrease substantially in the south and along the coasts. Zero crossing days will generally increase, most notably in colder regions.

Precipitation is expected to intensify, with more frequent wet days and more precipitation on these days across Svalbard. The number of very heavy precipitation days is projected to increase slightly, especially in eastern Spitsbergen. The fraction of autumn precipitation falling as snow is expected to decline in the southwest but remain dominant in the colder, glaciated regions of the northeast.

The study also provides specific projections for Longyearbyen and Ny-Ålesund, highlighting similar patterns of warming and precipitation increases. These local-scale insights are essential for understanding the potential impacts of climate change on both human settlements and ecological systems in Svalbard.

5 Dataset

An overview of available simulations is shown in Table 3. The data is freely available for download under the following URL:
https://thredds.met.no/thredds/catalog/pcch-arctic/catalog.html
The file format used is NetCDF and the variable names mostly follow the specifications set by CORDEX[1].

Table 3 Available simulations.

Simulation name	Input data	Scenario	Time period	Domain (see Fig. 1)	Nesting
HCLIM43_AROME_MPIESM12LR_SV25	MPI-ESM1-2-LR r1i1p1f1	SSP5-8.5	1991–2070	Svalbard 2.5 km	From 12 km ALADIN
HCLIM43_ALADIN_MPIESM12LR			1991–2070	Larger 12 km	No
HCLIM43_AROME_NorESM2MM_SV25	NorESM2-MM r1i1p1f1		1991–2070	Svalbard 2.5 km	From 12 km ALADIN
HCLIM43_ALADIN_NorESM2MM			1991–2070	Larger 12 km	No
HCLIM43_AROME_ERA5_SV25	ERA5	evaluation	2000–2024	Svalbard 2.5 km	No

[1] https://cordex.org/experiment-guidelines/cordex-cmip6/data-request-cordex-cmip6-rcms/

Acknowledgements

The work presented in this report was funded by the Norwegian Research Council, project "PCCH-Arctic", under grant ID 320769. The simulations were carried out on the Norwegian Research Infrastructure Services (NRIS) high-performance computing facility "Betzy", operated by Sigma2, under project number NN9875K.

References

Batrak, Y., & Müller, M. (2019). On the warm bias in atmospheric reanalyses induced by the missing snow over Arctic sea-ice. *Nature Communications, 10*(1), 4170.

Belušić, D., de Vries, H., Dobler, A., Landgren, O., Lind, P., Lindstedt, D., Pedersen, R. A., Sánchez-Perrino, J. C., Toivonen, E., van Ulft, B., Wang, F., Andrae, U., Batrak, Y., Kjellström, E., Lenderink, G., Nikulin, G., Pietikäinen, J.-P., Rodríguez-Camino, E., Samuelsson, P., van Meijgaard, E., & Wu, M. (2020). HCLIM38: a flexible regional climate model applicable for different climate zones from coarse to convection-permitting scales. *Geoscientific Model Development*, 13(3), 1311-1333.

Dobler, A., Lutz, J., Landgren, O., & Haugen, J. E. (2020). Circulation specific precipitation patterns over Svalbard and projected future changes. *Atmosphere*, *11*(12), 1378.

Førland, E. J., Skaugen, T. E., Benestad, R. E., Hanssen-Bauer, I. & Tveito, O. E. (2004). Variations in Thermal Growing, Heating, and Freezing Indices in the Nordic Arctic, 1900-2050. *Arctic, Antarctic and Alpine Research*, 36(3), 346-355.

Grünberg, I., Groenke, B., Westermann, S., & Boike, J. (2024). Permafrost and active layer temperature and freeze/thaw timing reflect climatic trends at Bayelva, Svalbard. *Journal of Geophysical Research: Earth Surface*, 129, e2024JF007648. https://doi.org/10.1029/2024JF007648

Hanssen-Bauer, I., Førland, E. J., Hisdal, H., Mayer, S., Sandø, A. B., & Sorteberget, A. (editors) (2019). Climate in Svalbard 2100 – a knowledge base for climate adaptation. *NCCS report* no. 1/2019, Norwegian Centre for Climate Services (NCCS), Oslo, Norway.

Hersbach, H., Bell, B., Berrisford, P., Hirahara, S., Horányi, A., Muñoz-Sabater, J., Nicolas, J., Peubey, C., Radu, R., Schepers, D., Simmons, A., Soci, C., Abdalla, S., Abellan, X., Balsamo, G., Bechtold, P., Biavati, G., Bidlot, J., Bonavita, M., De Chiara, G., Dahlgren, P., Dee, D., Diamantakis, M., Dragani, R., Flemming, J., Forbes, R., Fuentes, M., Geer, A., Haimberger, L.,

Meteorologisk institutt
Meteorological Institute
Org.no 971274042
post@met.no

Oslo
P.O. Box 43 Blindern
0313 Oslo, Norway
T. +47 22 96 30 00

Bergen
Allégaten 70
5007 Bergen, Norway
T. +47 55 23 66 00

Tromsø
P.O. Box 6314,
Langnes
9293 Tromsø, Norway
T. +47 77 62 13 00

www.met.no

Healy, S., Hogan, R. J., Hólm, E., Janisková, M., Keeley, S., Laloyaux, P., Lopez, P., Lupu, C., Radnoti, G., de Rosnay, P., Rozum, I., Vamborg, F., Villaume, S., & Thépaut, J. N. (2020). The ERA5 global reanalysis. *Quarterly Journal of the Royal Meteorological Society*, *146*(730), 1999-2049, https://doi.org/https://doi.org/10.1002/qj.3803

Isaksen, K., Nordli, Ø., Ivanov, B., Køltzow, M. A. Ø., Aaboe, S., Gjelten, H. M., Mezghani, A., Eastwood, S., Førland, E., Benestad, R. E., Hanssen-Bauer, I., Brækkan, R., Sviashchennikov, P., Demin, V., Revina, A., & Karandasheva, T. (2022). Exceptional warming over the Barents area. *Scientific Reports,* 12(9371). https://doi.org/10.1038/s41598-022-13568-5

Isaksen, K., Lutz, J., Macdonald Sørensen, A., Godøy, Ø., Ferrighi, L., Eastwood, S., & Aaboe, S. (2022). Advances in operational permafrost monitoring on Svalbard and in Norway. *Environmental Research Letters*, 17(9). https://doi.org/https://doi.org/10.1088/1748-9326/ac8e1c

Jaskólski, M. W., Pawłowski, Ł., & Strzelecki, M. C. (2018). High Arctic coasts at risk—the case study of coastal zone development and degradation associated with climate changes and multidirectional human impacts in Longyearbyen (Adventfjorden, Svalbard). *Land degradation & development*, 29(8), 2514-2524.

Levine, X. J., Williams, R. S., Marshall, G., Orr, A., Seland Graff, L., Handorf, D., Karpechko, A., Köhler, R.,Wijngaard, R. R., Johnston, N., Lee, H., Nieradzik, L. & Mooney, P. A. (2024). Storylines of summer Arctic climate change constrained by Barents–Kara seas and Arctic tropospheric warming for climate risk assessment. *Earth System Dynamics*, 15(4), 1161-1177. https://doi.org/10.5194/esd-15-1161-2024

Mauritsen, T., Bader, J., Becker, T., Behrens, J., Bittner, M., Brokopf, R., Brovkin, V., Claussen, M., Crueger, T., Esch, M., Fast, I., Fiedler, S., Fläschner, D., Gayler, V., Giorgetta, M., Goll, D., Haak, H., Hagemann, S., Hedemann, C., & Roeckner, E. (2019). Developments in the MPI-M Earth System Model version 1.2 (MPI-ESM 1.2) and its response to increasing CO2, *Journal of Advances in Modeling Earth Systems*, 11, https://doi.org/10.1029/2018MS001400

Onarheim, I. H., Eldevik, T., Smedsrud, L. H., & Stroeve, J. C. (2018). Seasonal and regional manifestation of Arctic sea ice loss. *Journal of Climate*, 31(12), 4917–4932. https://doi.org/10.1175/JCLI-D-17-0427.1

O'Neill, B. C., Tebaldi, C., Van Vuuren, D. P., Eyring, V., Friedlingstein, P., Hurtt, G., Knutti, R., Kriegler, E., Lamarque, J.-F., Lowe, J., Meehl, G. A., Moss, R., Riahi, K. & Sanderson, B. M. (2016). The scenario model intercomparison project (ScenarioMIP) for CMIP6. *Geoscientific Model Development*, *9*(9), 3461-3482.

Pedersen, Å. Ø., Convey, P., Newsham, K. K., Mosbacher, J. B., Fuglei, E., Ravolainen, V., Hansen, B. B., Jensen, T. C., Augusti, A., Biersma, E. M., Cooper, E. J., Coulson, S. J., Gabrielsen, G. W., Gallet, J. C., Karsten, U., Kristiansen, S. M., Svenning, M. M., Tveit, A. T., Uchida, M., Baneschi, I., Calizza, E., Cannone, N., de Goede, E. M., Doveri, M., Elster, J., Giamberini, M. S., Hayashi, K., Lang, S. I., Lee, Y. K., Nakatsubo, T., Pasquali, V., Paulsen, I. M. G., Pedersen, C., Peng, F., Provenzale, A., Pushkareva, E., Sandström, C. A. M., Sklet, V., Stach, A., Tojo, M., Tytgat, B., Tømmervik, H., Velazquez, D., Verleyen, E., Welker, J. M., Yao, Y. F., & Loonen, M. J. J. E. (2022). Five decades of terrestrial and freshwater research at Ny-Ålesund, Svalbard. *Polar Research*, 41(6310). https://doi.org/10.33265/polar.v41.6310

van **Pelt**, W. J. J., Schuler T. V., Pohjola, V. A., Pettersson, R. (2021). Accelerating future mass loss of Svalbard glaciers from a multi-model ensemble. *Journal of Glaciology,* 67(263), 485-499. https://doi.org/10.1017/jog.2021.2

Schyberg H., Yang X., Køltzow M.A.Ø., Amstrup B., Bakketun Å., Bazile E., Bojarova J., Box J. E., Dahlgren P., Hagelin S., Homleid M., Horányi A., Høyer J., Johansson Å., Killie M.A., Körnich H., Le Moigne P., Lindskog M., Manninen T., Nielsen Englyst P., Nielsen K.P., Olsson E., Palmason B., Peralta Aros C., Randriamampianina R., Samuelsson P., Stappers R., Støylen E., Thorsteinsson S., Valkonen T., Wang Z.Q., (2020). Arctic regional reanalysis on single levels from 1991 to present. *Copernicus Climate Change Service (C3S) Climate Data Store (CDS)*. DOI: https://doi.org/10.24381/cds.713858f6

Seland, Ø., Bentsen, M., Olivié, D., Toniazzo, T., Gjermundsen, A., Graff, L. S., Debernard, J. B., Gupta, A. K., He, Y.-C., Kirkevåg, A., Schwinger, J., Tjiputra, J., Aas, K. S., Bethke, I., Fan, Y., Griesfeller, J., Grini, A., Guo, C., Ilicak, M., Karset, I. H. H., Landgren, O., Liakka, J., Moseid, K. O., Nummelin, A., Spensberger, C., Tang, H., Zhang, Z., Heinze, C., Iversen, T., & Schulz, M. (2020) Overview of the Norwegian Earth System Model (NorESM2) and key climate response of CMIP6 DECK, historical, and scenario simulations, *Geoscientific Model Development*, 13, 6165–6200. https://doi.org/10.5194/gmd-13-6165-2020

Streletskiy, D. A., Clemens, S., Lanckman, J.-P., & Shiklomanov, N. I. (2023). The costs of Arctic infrastructure damages due to permafrost degradation. *Environmental Research Letters*, 18(1), 015006. https://doi.org/10.1088/1748-9326/acab18

Wang, F. (2024). An introduction to the HARMONIE-Climate (HCLIM) regional climate modeling system. *Zenodo*. https://doi.org/10.5281/zenodo.11424181

Meteorologisk institutt
Meteorological Institute
Org.no 971274042
post@met.no

Oslo
P.O. Box 43 Blindern
0313 Oslo, Norway
T. +47 22 96 30 00

Bergen
Allégaten 70
5007 Bergen, Norway
T. +47 55 23 66 00

Tromsø
P.O. Box 6314,
Langnes
9293 Tromsø, Norway
T. +47 77 62 13 00

www.met.no